Published on 19 January 2018. Downloaded by University of Science and Technology of China on 1/9/2023 9:29:17 AM.

ChemComm

COMMUNICATION

View Article Online
View Journal | View Issue

Check for updates

Cite this: *Chem. Commun.*, 2018, **54**, 1964

Received 1st December 2017,
Accepted 19th January 2018

DOI: 10.1039/c7cc09223g

rsc.li/chemcomm

Polyoxometalate-encapsulated twenty-nuclear silver-tetrazole nanocage frameworks as highly active electrocatalysts for the hydrogen evolution reaction†

Shaobin Li,‡[ab] Li Zhang,‡[a] Yaqian Lan,[c] Kevin P. O'Halloran,[d] Huiyuan Ma*[a] and Haijun Pang*[a]

Two unprecedented polyoxometalate-encapsulated twenty-nuclear silver-tetrazole nanocage frameworks have been synthesized, which exhibit high activity in hydrogen evolution reaction. HUST-100 shows an onset overpotential of 148 mV and a Tafel slope of 82 mV dec^{-1}, and the catalytic current density approaches 10 mA cm^{-2} at an overpotential of 234 mV.

Molecular hydrogen (H_2) has been advocated as the ideal energy carrier because it is a potential clean and renewable alternative for fossil fuels in the future.[1] The electrocatalytic reduction of water is considered to be the simplest way to produce hydrogen of high purity at the most economical price. The hydrogen evolution reaction (HER, $2H^+ + 2e^- \rightarrow H_2$) constitutes the second half of the water-splitting reaction.[2] The ideal catalysts for the HER should achieve a large exchange current and a small Tafel slope. Platinum (Pt) is the best known HER catalyst, but the high cost and limited global supply of Pt may hamper its use in a large scale commercial process.[3] The exploitation of inexpensive and effective catalysts is highly desirable to produce viable water electrolytic systems.

Metal–organic nanocages (MONCs) have a well-defined porous structure and are a special type of metal–organic frameworks (MOFs).[4] The permanent porosity and high surface area of MONCs may provide an advantage towards electrocatalytic reactions such as HER and oxygen reduction reaction (ORR).[5] However, it is difficult to intentionally construct MONCs structures due to the random coordination between the metal ions and organic ligands. In this regard, control of the assembly processes of constructing metal–organic nanocages is obviously a synthetic challenge. Recently, an important and effective synthesis strategy uses various anions such as halide anions, NO_3^-, BF_4^-, ClO_4^-, PF_6^-, and SO_4^{2-} as templates to direct the formation of MONCs (Scheme S1, ESI†).[6]

In this regard, POMs are a unique class of inorganic metal oxide clusters,[7] which can provide polyoxoanions as templates to direct the formation of MONCs. Compared with simple anionic templates, POMs display two advantages: (i) as a structural advantage, POMs exhibit a wide variety of shapes, sizes and high negative charges, directing the formation of various MONCs with adjustable sizes; and (ii) as a functionality advantage, POMs can participate in rapid reversible multi-electron transfer reactions. For instance, the Keggin POMs exhibit a reversible uptake of 24-electrons.[8] The fast, reversible multi-electron transfer demonstrated by POMs makes them well suited for HER catalysts, and several excellent studies hitherto utilizing POM-based MOFs (POMOFs) for HER applications have been reported.[9] However, after carefully searching the CSD database and previous literature, only rare examples of POMs as templates to direct the formation of MONCs were observed so far;[10] furthermore, the utilization of POM-templated MONCs for HER applications has not yet been investigated. Lu *et al.* made an important breakthrough in 2010, in which Keggin-type polyoxoanions played a template role to direct the formation of the silver-triazole (1,2,4-triazole) polycatenane framework with adamantine-like $[Ag_{24}(trz)_{18}]^{6+}$ nanocages.[10a] Inspired by this successful example, we sought to introduce Keggin-type polytungstates into a silver-tetrazole framework to construct new POM-encapsulated MONCs structures and provide a new model for HER applications. Compared to other azolates with fewer N-donors, tetrazolate (tta) not only has the highest number of N-donors, but it also has versatile coordination modes (Scheme S2, ESI†). Classic examples of the μ_4 bonding mode for tetrazolate have been observed in $[Ag_{1.5}(\mu_4\text{-tta})]\text{-}(NO_3)_{0.5}$

[a] *Key Laboratory of Green Chemical Engineering and Technology of College of Heilongjiang Province, College of Chemical and Environmental Engineering, Harbin University of Science and Technology, Harbin, 150040, P. R. China. E-mail: mahy017@163.com, panghj116@163.com*

[b] *Key Laboratory of Polymeric Composite Materials of Heilongjiang Province, College of Materials Science and Engineering, Qiqihar University, Qiqihar, 161006, P. R. China*

[c] *College of Chemistry and Materials Science, Nanjing Normal University, Nanjing 210023, P. R. China*

[d] *School of Science and Technology, Georgia Gwinnett College, Lawrenceville, GA 30043, USA*

† Electronic supplementary information (ESI) available: Experimental details, additional characterization data, tables, and figures. CCDC 1588388 and 1588233. For ESI and crystallographic data in CIF or other electronic format see DOI: 10.1039/c7cc09223g

‡ These authors contributed equally to this work.

This journal is © The Royal Society of Chemistry 2018

Published on 19 January 2018. Downloaded by University of Science and Technology of China on 1/9/2023 9:29:17 AM.

as reported by Ciani *et al.*[11] and [Cu(μ_4-tta)] as reported by Zhang *et al.*[12] These discoveries led us to use these frameworks with polyoxometalate systems.

Herein, the isolation of two novel 3D silver-tetrazole frameworks with unprecedented $[Ag_{20}(tta)_{16}]^{4+}$ nanocage encapsulated 24-connected POMs is described, namely, $Ag_{10}(\mu_4\text{-tta})_4(H_2O)_4(PW_9^{VI}W_3^{V}O_{40})$ (**HUST-100**) and $Ag_{10}(\mu_4\text{-tta})_4(H_2O)_4(SiW_{10}^{VI}W_2^{V}O_{40})$ (**HUST-101**) (HUST = Harbin University of Science and Technology; tta = tetrazolate). It should be pointed out that **HUST-100** and **HUST-101** represent the first examples of 3D POM-encapsulated silver-tetrazole frameworks with twenty-nuclear $[Ag_{20}(tta)_{16}]^{4+}$ nanocages. More importantly, 24-connected POMs exhibit the highest connection numbers in POM-based hybrids to date. This work is additional evidence to authenticate that POMs could play a template role to direct the formation of MONCs. Furthermore, the electrocatalytic activities of the as-synthesized **HUST-100** and **HUST-101** toward HER were examined in acidic aqueous solution (0.5 M H_2SO_4). As a novel, non-noble-metal HER catalyst in acidic media, **HUST-100** shows high activity with a Tafel slope of 82 mV dec^{-1} and an exchange current density of 0.011 mA cm^{-2}, which needs an overpotential (η) of 234 mV to attain a current density of 10 mA cm^{-2}.

The red block crystals of **HUST-100** and **HUST-101** were obtained from the reaction of the Keggin-type POMs ($H_3PW_{12}O_{40}$ and $H_4SiW_{12}O_{40}$), $AgNO_3$, tetrazolate and 1,3,5-benzenetricarboxylate in water under hydrothermal reaction conditions (Fig. S1, ESI†). Although 1,3,5-benzenetricarboxylate is not part of the final structure, it's use is necessary in the synthesis as the title compounds cannot be obtained without it. Single crystal X-ray diffraction (ESI†) reveals that **HUST-100** and **HUST-101** are isomorphous crystals with the tetragonal space group *I*4*m*2 (no. 119). The Keggin-type POMs ($H_3PW_{12}O_{40}$ and $H_4SiW_{12}O_{40}$) have been introduced into a 20-nuclear silver nanocage framework as guests. Therefore, only the structure of **HUST-100** is described for brevity. The asymmetric unit of **HUST-100** consists of one $[PW^{IV}{}_9W^{V}{}_3O_{40}]^{6-}$ polyanion (abbreviated as $PW_{12}O_{40}$), ten silver ions, four deprotonated tta ligands and four coordinated water molecules (Fig. S2, ESI†). The reduced-polyanion $PW_{12}O_{40}$ shows a classic Keggin-type structure and possesses a higher charge density than common oxidized Keggin polyanion, which makes them favourable for forming a highly connected framework.

There are three crystallographically independent silver cations (Ag1, Ag2 and Ag3) with two kinds of coordination modes (Fig. S3, ESI†). Both Ag1 and Ag2 cations adopt a similar tetra-coordinated "seesaw-shape" geometry, which is coordinated by two nitrogen atoms from two tta ligands, and two oxygen atoms from two $PW_{12}O_{40}$ polyoxoanions. The Ag3 cation is coordinated by four water molecules, two terminal oxygen atoms from two $PW_{12}O_{40}$ clusters and one silver atom [Ag3–Ag3 = 2.97 Å], forming a $\{Ag\text{–}Ag\}^{2+}$ aggregate (Fig. S3, ESI†). It should be pointed out that the distance between two adjacent silver atoms (2.97 Å) is much shorter than the van der Waals contact distance of silver atoms (3.44 Å), and longer than the sum of their covalent radius contact distance between silver and oxygen atoms (2.27 Å).[13] The bond lengths of Ag–N (1.918–2.082 Å) are within the normal range of silver-nitrogen compounds. The tta ligand is deprotonated during the reaction, and each tta ligand is attached to four Ag atoms in a μ_4-coordination fashion (Fig. S3, ESI†). Thus, four silver cations are linked with four tta ligands to generate two kinds of $[Ag_4(tta)_4]$ macrocycles (Fig. S4, ESI†). The windows of macrocycle A and B are about 4.81 × 4.81 Å and 7.29 × 7.29 Å, respectively. Each macrocycle A is linked with four macrocycle B, and each macrocycle B is linked with four macrocycle A. Interestingly, a novel three dimensional silver-tetrazole host framework is formed by this alternate connection mode. From a topological view, if the tta ligands are considered as 4-connected nodes, this host framework is considered as a 4-connected net. Simplifying further, the topology of the host framework is a classical **dia** net (Fig. S5, ESI†).

A prominent structural feature of the host framework is the presence of an unprecedented vase-like nanocage built from 20 Ag centers and 16 tta ligands (Fig. 1 and Fig. S6, ESI†). Clearly the diameter of the nanocage is suitable to encapsulate the Keggin polyoxoanion (~10.5 Å). Finally, the polyoxoanion acts as a 24-connected inorganic template which is encapsulated into a vase-like $[Ag_{20}(tta)_{16}]^{4+}$ nanocage host framework (Fig. 1b and c). Meanwhile, these adjacent polyoxoanions are further fused together by four Ag–O bonds from the $\{Ag\text{–}Ag\}^{2+}$ aggregates, which integrally stabilize the nanocage framework (Fig. S7, ESI†). A most remarkable structural feature is that **HUST-100** represents the first example of a 3D silver-tetrazole framework with a $[Ag_{20}(tta)_{16}]^{4+}$ nanocage. More importantly, 24-connected POMs exhibit the highest connection numbers in POM-based hybrids to date.

From a topological view, if the tta ligands and {Ag3–Ag3} aggregates are regarded as 4-connected nodes, and the Keggin POM clusters as a 24-connected node, the structure of **HUST-100** can be considered as a 3D (4,4,24)-connected framework, which exhibits a novel topology (Fig. S8, ESI†). It should be pointed out that this Keggin POM cluster is the second real 24-connected node, which is an important discovery in topological crystal chemistry.[14] Offering further insight into this intricate architecture, if each POM-encapsulated $[Ag_{20}(tta)_{16}]^{4+}$ nanocage is considered as a

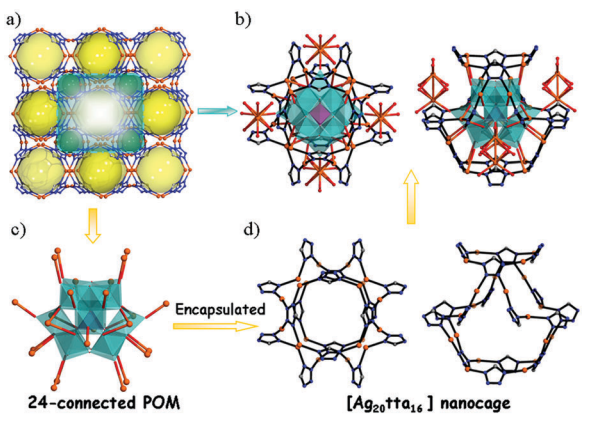

Fig. 1 (a) The 3D POM-encapsulated 20-nuclear nanocage framework in **HUST-100**; (b) the structure of the POM-encapsulated nanocage; (c) the 24-connected POM cluster; (d) the structure of the 20-nuclear $[Ag_{20}(tta)_{16}]^{4+}$ nanocage.

Published on 19 January 2018. Downloaded by University of Science and Technology of China on 1/9/2023 9:29:17 AM.

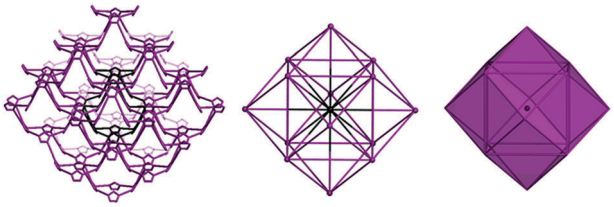

Fig. 2 Schematic view of the 14-connected POM-encapsulated $[Ag_{20}(tta)_{16}]$ nanocage uninodal framework and a dodecahedron coordination figure.

14-connected node, the overall structure of **HUST-100** can also be considered as a uninodal 14-connected framework. Each POM-encapsulated $[Ag_{20}(tta)_{16}]^{4+}$ nanocage has a dodecahedron coordination figure which is enclosed by fourteen adjacent POM-encapsulated $[Ag_{20}(tta)_{16}]^{4+}$ nanocages (Fig. 2 and Fig. S9, ESI†). Attempts have been made to use other types of POMs (such as Dawson-type, Anderson-type, and Lindqvist-type) to construct this framework. However, the framework could not be maintained with other types of POMs under the same conditions. This indicates that Keggin-type POMs are efficient templates for the *in situ*-formation of porous frameworks due to their quasi-spherical architecture and suitable size.

A high structural stability is key to some applications of materials. The phase purities of **HUST-100** and **HUST-101** were established by comparing their observed and simulated powder X-ray diffraction (PXRD) patterns. **HUST-100** and **HUST-101** are air-stable, maintaining their crystallinities for at least several months, with no observed efflorescence. Furthermore, **HUST-100** and **HUST-101** are stable in acidic aqueous solutions in the pH range of 1–7 at room temperature, as confirmed by the subsequent IR and PXRD measurements (Fig. S11 and S12, ESI†). As highly active HER catalysts, POM-based hybrid materials should be stable in acidic media.

The HER catalytic activities of as-synthesized **HUST-100** and **HUST-101** were also evaluated by electrochemical experiments. Fig. 3a shows the HER polarization curves of electrocatalysts in 0.5 M H_2SO_4 aqueous solution with a scan rate of 5 mV s^{-1}, including those of **HUST-100** and **HUST-101**-modified electrodes with different loading amounts (20 wt%, 50 wt%, as well as pure crystals), and commercial Pt/C (20 wt% Pt/XC-72R). The HER activities of **HUST-100** and **HUST-101**-modified electrodes are enhanced after carbon black doping. These results demonstrate that the HER activity of POM-encapsulated MOF-modified electrodes mainly originates from the synergistic effect between the POM-encapsulated MOF material and carbon black. After careful analysis of these results, we infer that the title compounds may contribute to the low overpotential, and carbon black contributes to the high current density. It is necessary to dope carbon black into POM-encapsulated MOF, which not only improves the electrical conductivity but also increases the current. Increasing the content of the title compounds in the composite electrode facilitates charge transfer to some extent and thereby results in improved HER activity. For instance, the composite with 50 wt% title compounds exhibit better catalytic behavior than the composite with 20 wt% title compounds. The **HUST-100** (50 wt%) shows an onset potential of 148 mV and a Tafel slope of

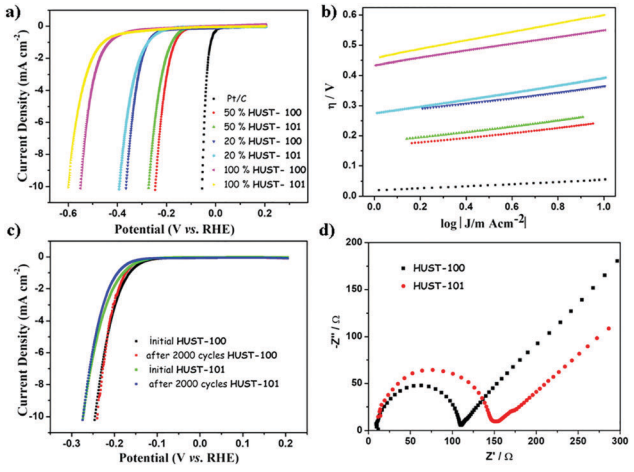

Fig. 3 (a) Polarization curves of **HUST-100** and **HUST-101**-doped composites with different loadings in 0.5 M H_2SO_4 aqueous solution; (b) the corresponding Tafel plots; (c) polarization curves of **HUST-100** and **HUST-101** (50 wt%) initially in 0.5 M H_2SO_4 aqueous solution and after 2000 cycles; and (d) electrochemical impedance spectroscopy (EIS) Nyquist plots of **HUST-100** and **HUST-101** (50 wt%).

82 mV dec^{-1}. As expected, among all tested electrodes, Pt/C exhibits the highest activity for HER with nearly zero onset overpotential (η) and a high current density. Pure XC-72R has negligible electrocatalytic activity, while the doped samples may enhance the HER activity by the introduction of active sites. The **HUST-100**-modified electrode is highly active toward HER, and it approaches a large current density of 10 mA cm^{-2} at an overpotential of 234 mV. The required overpotentials for driving a current of 10 mA cm^{-2} (η_{10}) is more practical owing to the fact that a solar light-coupled HER apparatus usually runs at 10–20 mA cm^{-2} under standard conditions, indicating that 10 mA cm^{-2} is meaningful as the point of reference.[2b] According to previous reports,[9b] the modified electrodes **NENU-500**, **NENU-501**, **ε(trim)4/3**, **NENU-499**, **NENU-5** and **HKUST-1** require an overpotential of 237, 392, 515, 570, 585 and 691 mV, respectively, to achieve a 10 mA cm^{-2} HER current density (Table S3, ESI†). These six reported MOF composite electrodes exhibit larger overpotentials (η_{10}) than that of the **HUST-100** composite electrode, suggesting that fast and efficient electron transfer occurs on the **HUST-100** modified electrode. The results imply that **HUST-100** is superior in catalytic activity over the other six electrocatalysts.

Tafel slope is an inherent property of electrocatalytic materials, which is determined by the rate-limiting step of HER. Additionally, the determination and interpretation of Tafel slope are important for the elucidation of the HER mechanism involved. Fig. 3b displays the Tafel plots for **HUST-100** and **HUST-101**-doped composites with different contents. The linear portions of the Tafel plots are fitted to the Tafel equation.[9e] Commercial Pt/C shows a Tafel slope of 30 mV dec^{-1} which is in agreement with the reported value.[15] The Tafel slopes of **HUST-100**, **HUST-101**, **NENU-500**, **NENU-501**, **ε(trim)4/3**, **NENU-499**, **NENU-5** and **HKUST-1** obtained from the Tafel plots are 82, 94, 96, 137, 142, 122, 94 and 127 mV dec^{-1}, respectively (Table S3, ESI†). The exchange current density (j_0) of **HUST-100** is calculated to be about 0.011 mA cm^{-2}. Compared with those non-noble-metal electrocatalytic materials reported

 This journal is © The Royal Society of Chemistry 2018

Published on 19 January 2018. Downloaded by University of Science and Technology of China on 1/9/2023 9:29:17 AM.

recently, the **HUST-100** electrode presents a quite large exchange current density and a relatively small Tafel slope,[16] suggesting that **HUST-100** is highly efficient for the kinetics of hydrogen evolution. A promising material for electrocatalytic HER should exhibit not only high activity but also good durability. Therefore, we also examined the stability of **HUST-100** and **HUST-101** in hydrogen generation by an accelerated degradation experiment. As shown in Fig. 3c, after continuous CV scanning for 2000 cycles in 0.5 M H_2SO_4 aqueous solution at a scan rate of 100 mV s^{-1}, the polarization curves show a negligible difference compared with the initial one. The result demonstrates that **HUST-100** and **HUST-101**-modified electrodes are durable during electrocatalytic hydrogen production. The time-dependent current density curves of **HUST-100** and **HUST-101** show excellent long-term stability (Fig. S13, ESI†). Electrochemical impedance spectroscopy (EIS) analysis was also performed to investigate the activity of **HUST-100** and **HUST-101** toward HER. Fig. 3d exhibits the obtained charge transfer resistance (R_{ct}). R_{ct} values of 100.4 Ω and 135.3 Ω were obtained for **HUST-100** and **HUST-101** (loading amounts of 50 wt%), respectively. This lower value for **HUST-100** validates the higher electrocatalytic activity for HER.

In conclusion, two novel POM-encapsulated silver-tetrazole nanocage frameworks, **HUST-100** and **HUST-101**, were synthesized, which represent the first examples of 3D silver-tetrazole frameworks with 20-nuclear $[Ag_{20}(tta)_{16}]^{4+}$ nanocages. More importantly, 24-connected POMs exhibit the highest connection numbers in POM-based materials to date. Furthermore, **HUST-100** and **HUST-101** exhibit not only good air stability but also acid tolerance. Therefore, **HUST-100** and **HUST-101**, as POM-based materials, were utilized as electrocatalysts toward HER, owing to the combination of the redox activity of POM moieties and the porosity of MONCs. Remarkably, **HUST-100** is highly active for electrochemically generating hydrogen from water under acidic conditions, with a Tafel slope of 82 mV dec^{-1} and an exchange current density of 0.011 mA cm^{-2}. The present study not only demonstrates a successful case to construct stable POM-encapsulated MONCs but also provides novel hydrogen-evolving electrocatalysts with excellent activity. Further investigation is currently underway in our group.

This work was financially supported by the National Science Foundation of China (21671049, 51572063, 21371041 and 21603113), and the National Science Foundation of Heilongjiang Province (QC2016014).

Conflicts of interest

There are no conflicts to declare.

Notes and references

1 (*a*) M. S. Dresselhaus and I. L. Thomas, *Nature*, 2001, **414**, 332–337; (*b*) J. A. Turner, *Science*, 2004, **305**, 972–974.
2 (*a*) E. Antolini, *Energy Environ. Sci.*, 2009, **2**, 915–931; (*b*) M. G. Walter, E. L. Warren, J. R. McKone, S. W. Boettcher, Q. Mi, E. A. Santori and N. S. Lewis, *Chem. Rev.*, 2010, **110**, 6446–6473; (*c*) Z. W. Seh, J. Kibsgaard, C. F. Dickens, I. B. Chorkendorff, J. K. Norskov and T. F. Jaramillo, *Science*, 2017, **355**, eaad4998.
3 L. Han, S. J. Dong and E. K. Wang, *Adv. Mater.*, 2016, **28**, 9266–9291.
4 (*a*) G. Férey, C. Mellot-Draznieks, C. Serre, F. Millange, J. Dutour, S. Surblé and I. Margiolaki, *Science*, 2005, **309**, 2040–2042; (*b*) H. C. Zhou, J. R. Long and O. M. Yaghi, *Chem. Rev.*, 2012, **112**, 673–674.
5 (*a*) M. Jahan, Z. Liu and K. P. Loh, *Adv. Funct. Mater.*, 2013, **23**, 5363–5372; (*b*) Q. H. Yang, Q. Xu and H. L. Jiang, *Chem. Soc. Rev.*, 2017, **46**, 4774–4808.
6 (*a*) L. Chen, Q. H. Chen, M. Y. Wu, F. L. Jiang and M. C. Hong, *Acc. Chem. Res.*, 2015, **48**, 201–210; (*b*) R. Custelcean, *Chem. Soc. Rev.*, 2014, **43**, 1813–1824; (*c*) J. D. Pang, F. L. Jiang, D. Q. Yuan, J. Zheng, M. Y. Wu, G. L. Liu, K. Z. Su and M. C. Hong, *Chem. Sci.*, 2014, **5**, 4163–4166.
7 (*a*) Y. C. Huang, J. W. Zhang, J. X. Ge, C. Sui, J. Hao and Y. G. Wei, *Chem. Commun.*, 2017, **53**, 2551–2554; (*b*) G. G. Gao, F. Y. Li, L. Xu, X. Z. Liu and Y. Y. Yang, *J. Am. Chem. Soc.*, 2008, **130**, 10838–10839; (*c*) L. Huang, S. S. Wang, J. W. Zhao, L. Cheng and G. Y. Yang, *J. Am. Chem. Soc.*, 2014, **136**, 7637–7642; (*d*) R. Tsunahima, C. Richmond and L. Cronin, *Chem. Sci.*, 2012, **3**, 343–348.
8 H. Wang, S. Hamanaka, Y. Nishimoto, S. Irle, T. Yokoyama, H. Yoshikawa and K. Awaga, *J. Am. Chem. Soc.*, 2012, **134**, 4918–4924.
9 (*a*) B. Nohra, H. E. Moll, L. M. R. Albelo, P. Mialane, J. Marrot, C. Mellot-Draznieks, M. O'Keeffe, R. N. Biboum, J. Lemaire, B. Keita, L. Nadjo and A. dolbecq, *J. Am. Chem. Soc.*, 2011, **133**, 13363–13374; (*b*) J. S. Qin, D. Y. Du, W. Guan, X. J. Bo, Y. F. Li, L. P. Guo, Z. M. Su, Y. Y. Wang, Y. Q. Lan and H. C. Zhou, *J. Am. Chem. Soc.*, 2015, **137**, 7169–7177; (*c*) Y. J. Tang, M. R. Gao, C. H. Liu, S. L. Li, H. L. Jiang, Y. Q. Lan, M. Han and S. H. Yu, *Angew. Chem., Int. Ed.*, 2015, **54**, 1–6; (*d*) X. J. Yang, X. J. Feng, H. Q. Tan, H. Y. Zang, X. L. Wang, Y. H. Wang, E. B. Wang and Y. G. Li, *J. Mater. Chem. A*, 2016, **4**, 3947–3954; (*e*) Y. Y. Ma, C. X. Wu, X. J. Feng, H. Q. Tan, L. K. Yan, Y. Liu, Z. H. Kang, E. B. Wang and Y. G. Li, *Energy Environ. Sci.*, 2017, **10**, 788–798.
10 (*a*) X. F. Kuang, X. Y. Wu, R. M. Yu, J. P. Donahue, J. S. Huang and C. Z. Lu, *Nat. Chem.*, 2010, **2**, 461–465; (*b*) E. L. Zhou, C. Qin, X. L. Wang, K. Z. Shao and Z. M. Su, *Chem. – Eur. J.*, 2015, **21**, 1–8.
11 L. Carlucci, G. Ciani and D. M. Proserpio, *Angew. Chem., Int. Ed.*, 1999, **38**, 3488–3491.
12 X. M. Zhang, J. Lv, F. Ji, H. S. Wu, H. J. Jiao and P. R. Schleyer, *J. Am. Chem. Soc.*, 2011, **133**, 4788–4790.
13 P. P. Zhang, J. Peng, H. J. Pang, J. Q. Sha, M. Zhu, D. D. Wang, M. G. Liu and Z. M. Su, *Cryst. Growth Des.*, 2011, **11**, 2736–2742.
14 D. Y. Du, J. S. Qin, Z. Sun, L. K. Yan, M. O'Keeffe, Z. M. Su, S. L. Li, X. H. Wang, X. L. Wang and Y. Q. Lan, *Sci. Rep.*, 2013, **3**, 2616.
15 Y. G. Li, H. L. Wang, L. M. Xie, Y. Y. Liang, G. S. Hong and H. J. Dai, *J. Am. Chem. Soc.*, 2011, **133**, 7296–7299.
16 P. D. Tran, M. Nguyen, S. S. Pramana, A. Bhattacharjee, S. Y. Chiam, J. Fize, M. J. Field, V. Artero, L. H. Wong, J. Loo and J. Barber, *Energy Environ. Sci.*, 2012, **5**, 8912–8916.